AIP Journal of Applied Physics

Thermal transport across graphene and single layer hexagonal boron nitride

Jingchao Zhang, Yang Hong, and Yanan Yue

Citation: Journal of Applied Physics **117**, 134307 (2015); doi: 10.1063/1.4916985
View online: http://dx.doi.org/10.1063/1.4916985
View Table of Contents: http://scitation.aip.org/content/aip/journal/jap/117/13?ver=pdfcov
Published by the AIP Publishing

Thermal transport across graphene and single layer hexagonal boron nitride

Jingchao Zhang,[1,a)] Yang Hong,[2] and Yanan Yue[3,a)]
[1]Holland Computing Center, University of Nebraska-Lincoln, Lincoln, Nebraska 68588, USA
[2]Department of Chemistry, University of Nebraska-Lincoln, Lincoln, Nebraska 68588, USA
[3]School of Power and Mechanical Engineering, Wuhan University, Wuhan, Hubei 430072, China

(Received 26 January 2015; accepted 26 March 2015; published online 7 April 2015)

As the dimensions of nanocircuits and nanoelectronics shrink, thermal energies are being generated in more confined spaces, making it extremely important and urgent to explore for efficient heat dissipation pathways. In this work, the phonon energy transport across graphene and hexagonal boron-nitride (*h*-BN) interface is studied using classic molecular dynamics simulations. Effects of temperature, interatomic bond strength, heat flux direction, and functionalization on interfacial thermal transport are investigated. It is found out that by hydrogenating graphene in the hybrid structure, the interfacial thermal resistance (*R*) between graphene and *h*-BN can be reduced by 76.3%, indicating an effective approach to manipulate the interfacial thermal transport. Improved in-plane/out-of-plane phonon couplings and broadened phonon channels are observed in the hydrogenated graphene system by analyzing its phonon power spectra. The reported *R* results monotonically decrease with temperature and interatomic bond strengths. No thermal rectification phenomenon is observed in this interfacial thermal transport. Results reported in this work give the fundamental knowledge on graphene and *h*-BN thermal transport and provide rational guidelines for next generation thermal interface material designs. © *2015 AIP Publishing LLC*.
[http://dx.doi.org/10.1063/1.4916985]

I. INTRODUCTION

Graphene continues receiving extensive attentions due to its unique properties. Both experimental and theoretical analyses have been conducted to understand the unique thermal properties of suspended graphene under various conditions.[1–3] Hexagonal boron nitride (*h*-BN), which has two-dimensional (2D) sp^2 honeycomb structures similar to that of graphene, has recently attracted much attention because of its excellent mechanical strength and thermal properties.[4–7] Emergence of 2D materials with atomic-layer structures, such as graphene, *h*-BN, MoS_2, and WSe_2, which have excellent physical properties, provides an opportunity of substituting silicon-based micro/nano-electronics. An important issue before large-scale applications of these materials is their heat dissipation performance, especially when they are supported on a substrate, as in most scenarios. The interface heat conduction becomes a major limiting factor for the related nanoscale thermal engineering, and thus, the understanding and control of the interfacial thermal resistance are crucial to the development of high performance graphene-based devices.

Thermal conductance across graphene interfaces has been studied in both experimental and simulation works. A very high interfacial thermal resistance of $5.30^{+0.46}_{-0.46} \times 10^{-5}$ K·m^2/W is observed by using the Raman thermometry under surface Joule heating.[8] The thermal contact resistance between graphene and SiO_2 (in a sandwiched structure) was measured at 5.6×10^{-9}–1.2×10^{-8} K·m^2/W using a differential 3ω method.[9] Interfacial thermal conductance in hybrid graphene/silicene structures was investigated using classic molecular dynamics (MD) simulation. The calculated thermal resistance ranges from 10^{-9} to 10^{-7} K·m^2/W depending on the system geometry and temperature.[10,11] Using nonequilibrium MD (NEMD) simulation, Wei *et al.*[12] calculated the interfacial thermal resistance between two neighboring graphene layers at $\sim 4 \times 10^{-9}$ K·m^2/W.

Stacked 2D materials have attracted much attention with the emerging demand for high performance thermal interface materials (TIMs). Thermal transport in these low dimensional materials can be affected by various factors such as temperature, coupling strength, heat flux direction, and chemical functionalization. With growing system temperatures, both the phonon population and active phonon frequency range will increase, leading to a reduced phonon mean free path and stronger three-phonon scattering. Thermal conductivities (κ) of graphene and *h*-BN are reported to share the same non-monotonic trends with temperature, i.e., increase at low temperatures and decrease at high temperatures.[13–15] Thermal rectification is also an important mechanism to be taken into account for future thermal interface material design. It has been observed in various structures with geometrical and material asymmetry.[16,17] Thermal rectification of more than 20% has been found at carbon nanotube/graphene and silicon interfaces.[18] Functionalization leads to tunable electronic properties of graphene by opening its energy gap originated from carbon atom hybridizations, making it a promising material for thermoelectric applications. Understanding the effects of functionalization on interfacial thermal transport is critical and urgent before large-scale implementations.

In this work, phonon energy transport across stacked graphene nanoribbon (GNR) and *h*-BN interfaces are studied using classic MD simulations. Dependency of interfacial

a)Authors to whom correspondence should be addressed. Electronic addresses: zhang@unl.edu and yyue@whu.edu.cn

thermal resistance on temperature, interatomic bond strength, heat flux direction, and hydrogenation are investigated, respectively. Instead of using traditional NEMD method, a transient heating technique is applied to characterize the interfacial thermal resistance. After the hybrid system reaches steady state, an ultrafast heat impulse is uniformly imposed on the graphene system to follow the principles in the experimental laser heating process. The GNR's energy and temperatures are recorded after the excitation for R evaluations. Compared to the NEMD method, this transient heating technique is focused on the dynamic thermal response of the system and can greatly reduce the computation time. Modellings of the MD system and methodologies are discussed in the following paragraphs. Section III demonstrates the calculation results along with detailed analyses.

II. MODELLING

MD simulations in this work are performed using the large-scale atomic/molecular massively parallel simulator (LAMMPS) package.[19] The second generation of Brenner potential:[20] reactive empirical bond-order (REBO), based on the Tersoff potential[21,22] with interactions between C-C bonds is employed to model the GNR system. The REBO potential is employed because its functions and parameters are known to give reasonable predictions for the thermal properties of graphene, whereas the adaptive intermolecular reactive empirical bond-order (AIREBO) was reported underestimating the dispersion of ZA phonons in graphene.[23] Atomic interactions in the BN structure are described by the Tersoff potential developed by Sevik *et al.*[4,5,24] The C-BN couplings are modeled as van der Waals (vdW) interactions using the Lennard-Jones (LJ) potential $V(r) = 4\chi\varepsilon[(\sigma/r)^{12} - (\sigma/r)^{6}]$, where σ is the distance parameter, ε is the energy parameter, and r is the interatomic distance. Parameter χ is used to adjust the interaction strength between graphene and h-BN. The LJ parameters are calculated from the universal force field (UFF),[25] where $\varepsilon_{BC} = 5.964$ meV, $\sigma_{BC} = 3.533$ Å, $\varepsilon_{NC} = 5.964$ meV, and $\sigma_{NC} = 3.533$ Å.

To model the GNR/h-BN bilayer heterostructure, the GNR is stacked 3.86 Å above the h-BN monolayer. Configuration of the hybrid structure is depicted in Fig. 1. Periodic boundary conditions are applied in the lateral (x, y) directions and free boundary condition is applied in the out-of-plane (z) direction. An integration time step of 0.1 fs (1 fs $= 10^{-15}$ s) is used in all calculations. The bond lengths of graphene and h-BN are 1.42 Å and 1.45 Å, corresponding to lattice constants of $\alpha_{GNR} = 2.46$ Å and $\alpha_{h-BN} = 2.51$ Å, respectively.[26,27] The supercell consists of one GNR and one

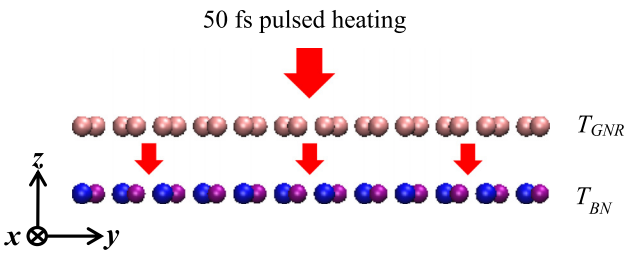

FIG. 1. Atomic configuration of the GNR and h-BN hybrid system.

h-BN lattice. Therefore, the modified lattice constant is calculated as $\alpha = (\alpha_{GNR} + \alpha_{h-BN})/2 = 2.485$ Å, which causes a lattice mismatch of 1% for both GNR and h-BN. A comparable lattice mismatch of 1.9% for graphene and MoS_2 monolayer has been proved by Ma *et al.*[28] using *ab initio* calculations. Compared with other graphene-based hybrid systems from the previous studies,[29–33] this lattice mismatch has negligible effects on the heterostructure's thermal properties.

A transient MD simulation approach is applied in this work to follow the principles of the experimental pump-probe technique, which is an optical thermal characterization method that has been used extensively for thermal characterization of micro/nanofilms.[34] The principle is to use a pump (pulsed) laser to introduce a short heating pulse. After that, the sample experiences a fast and small temperature rise due to the laser absorption and a slow temperature drop due to the heat dissipation down to the substrate. A probe laser is adopted to measure surface temperature simultaneously during/after the heating by probing the reflectance of laser beam which is temperature dependent. Initially, the GNR/h-BN hybrid structure is placed in canonical ensemble (NVT) at temperature 50 K for thermal equilibrium calculations of 1 ns (1 ns $= 10^{-9}$ s). Then another 1 ns microcanonical ensemble (NVE) calculations are performed for system relaxations. After the hybrid system reaches steady state, an ultrafast heat impulse is imposed on the GNR for 50 fs. In the heating process, non-translational kinetic energy is evenly added to the GNR system in each direction by rescaling velocities of atoms. As is shown in Fig. 2(a), when the excitation is released, the temperature of the GNR (T_{GNR}) increases dramatically and then gradually reduces during the thermal relaxation process. T_{GNR}, T_{BN}, and GNR system energy (E_t) are recorded each time step during the thermal relaxation. Physical meanings of the profiles in Fig. 2(a) are illustrated in the results and discussions session.

During the interfacial thermal transport process, the energy decay of GNR is caused by its thermal energy loss to the h-BN system. Therefore, given the energy and temperature evolutions of the GNR system, the interfacial thermal resistance between GNR/h-BN can be calculated using the equation

$$\partial E_t/\partial t = \mathrm{A} \cdot (T_{GNR} - T_{BN})/\mathrm{R}, \tag{1}$$

where E_t is the system energy of the supported GNR and A is GNR's area. An instant R can be calculated at each time step according to the local energy changing rate and corresponding temperature difference. We have tried this method and found it subject to the noise in the energy decay and the calculated interfacial thermal resistance has very large uncertainty. If R has little variation within the temperature range during thermal relaxation, a constant R value can be substituted into Eq. (1) to predict the E_t profile. Under such scenario, the interfacial thermal resistance can be calculated by the best fitting of the E_t profile using least square method. An alternative approach is to fit the temperature decay curve of GNR according to the lumped heat-capacity model $R = A\tau/C_v$, where A is the interface area, τ is the thermal

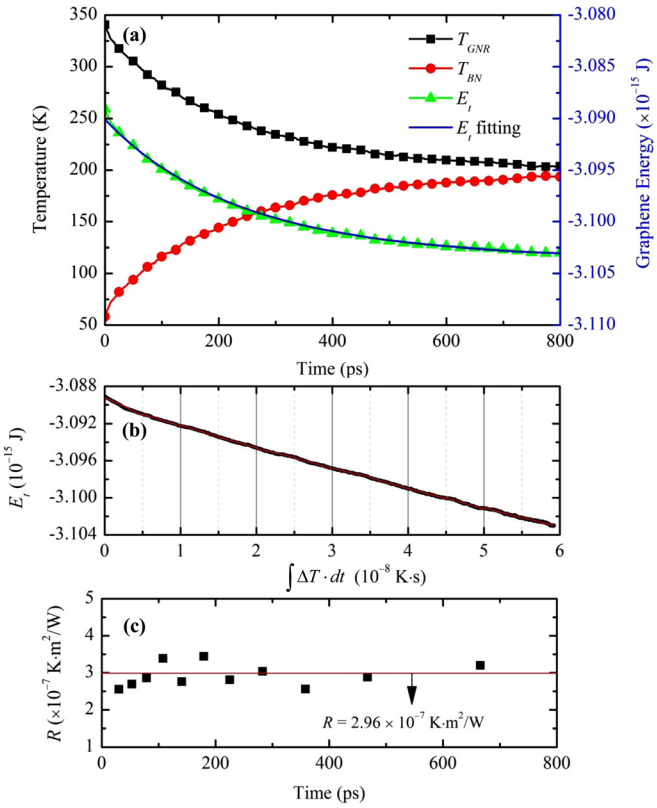

FIG. 2. (a) Temperature evolutions of GNR and *h*-BN after the ultrafast heat pulse are shown on the left *y*-axis; total energy of the GNR system and its fitting curve are shown on the right *y*-axis. (b) Energy relaxation profile of GNR can be correlated to $\Delta T dt$ by integrating the temperature differences between GNR and *h*-BN. (c) Segment interfacial thermal resistance values calculated from (b) are around the overall fitting results.

relaxation time, and C_v is the effective constant volume heat capacity of the hybrid system. Liu *et al.*[11] proved that the specific heat of graphene varies by no more than 7% within the temperature range of 300–500 K. Most of the previous studies regarded specific heat as a constant for interfacial thermal conductance calculations at different temperatures.[35–37] Thus, it is reasonable to treat R as a constant and use it in Eq. (1) for energy fitting. In this work, the energy decay method is preferred because the latter approach needs the knowledge of GNR's specific heat.

III. RESULTS AND DISCUSSIONS

A. Interfacial thermal resistance *R*

To investigate the interfacial thermal resistance between GNR and *h*-BN, a hybrid structure of dimensions 10.6 $\times$ 6.1 nm^2 ($x \times y$) is created. After the system reaches steady state under successive NVT and NVE calculations, a thermal impulse $\dot{q_{in}} = 6.16 \times 10^{-4}$ W is added to the GNR system to follow the principle of the laser irradiation in experimental studies. Temperatures of the GNR and *h*-BN are 340 K and 58 K, respectively, at the end of excitation. A relatively large difference (ΔT) between T_{GNR} and T_{BN} is necessary for stable temperature evolutions and $\Delta T \geq 200$ K is found proper in this study. Another 800 ps is run for data collection and the results are averaged by 100 in the calculation to suppress data noise. Final temperature of the system is determined as the steady state temperature after thermal relaxation. Temperature evolutions and energy fitting results are shown in Fig. 2(a). It is observed that after the 50 fs thermal excitation is released, the GNR's energy E_t drops quickly due to the heat transfer to *h*-BN. In the meantime, T_{GNR} goes down accordingly and a temperature rise is observed for the *h*-BN system. The energy decay fitting in Fig. 2(a) is performed based on Eq. (1) and takes the integral form of $E_t = E_0 + (R/A) \cdot \int_0^t (T_{GNR} - T_{BN}) dt$. Here, R is treated as a constant, and such assumption will be discussed and validated later. E_0 is graphene's initial energy.

The calculated interfacial thermal resistance at 200 K (R_{200K}) is 2.96×10^{-7} K·m^2/W, which is very close to the previous experimental results on thermal interface conductance across GNR/*h*-BN heterojunction.[38] At the beginning of the thermal relaxation process, a faster decay in GNR's total energy is observed. This is caused by the strong energy disturbance induced by the thermal impulse to the system. During that period, the potential and kinetic energies have not yet reached equilibrium. It can be observed from Fig. 2(a) that the fitting curve soundly matches the energy profile using a constant R_{200K}. This leads to a strong point that the interfacial thermal resistance between GNR and *h*-BN does not have large change over the relaxation temperature. As the energy decay is driven by the temperature difference $\Delta T = (T_{GNR} - T_{BN})$ as shown in Fig. 2(b), the graphene energy changes against $\int \Delta T dt$ is plotted. It is observed that the E_t profile has a linear relationship with $\int \Delta T dt$. In fact, we can use this profile to determine the interfacial thermal resistance. The E_t profile is divided into many segments as shown in Fig. 2(b). For each segment (t_1 to t_2), R can be treated as a constant and can be determined by linear fitting of the curve in Fig. 2(b). The fitted slope equals A/R, and can be used to determine R. The calculated results are shown in Fig. 2(c). It is observed that instant R values vary around the overall fitting results R_{200K}. Therefore, it is conclusive that the thermal resistance is constant during the transient process.

B. Effects of temperature and interface coupling strength

Graphene based TIMs are used to minimize the thermal resistance between different surfaces and are expected to work at various hot-spot temperatures. Figure 3(a) shows the interfacial thermal resistances from temperatures 200 K to 700 K calculated for three different LJ scaling parameters. It is observed that R decreases with temperature and interface coupling strength. Reportedly, compared with vdW bonding, the covalent bonding in graphene based TIMs can greatly reduce the thermal contact resistance, which indicates the stronger interatomic interactions are more effective for phonon transport across the interfaces.[8,39] The decrease in the thermal contact resistance with interface coupling strength χ can be explained from two aspects: (1) the phonon coupling between GNR and *h*-BN is enhanced, which directly reduces the interfacial thermal resistance and (2) the in-plane and out-of-plane phonons coupling in GNR become stronger, which indirectly boosts the efficiency of heat transfer from

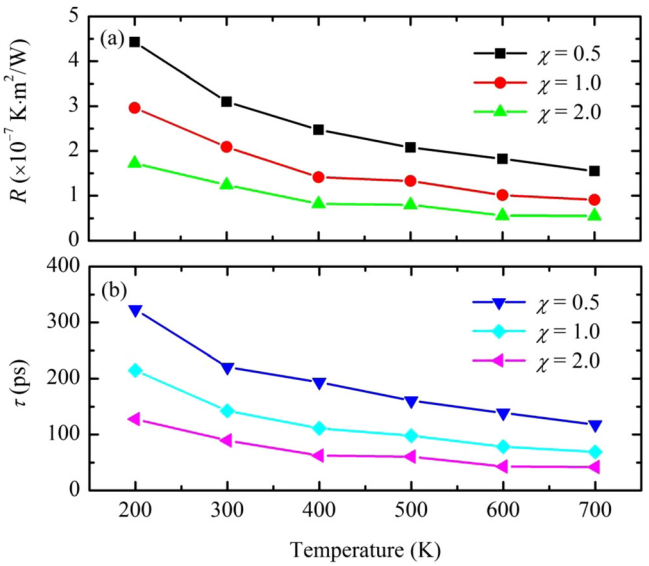

FIG. 3. (a) Thermal resistance R and (b) thermal relaxation time τ at different temperatures for LJ parameters $\chi = 0.5$, 1.0, and 2.0.

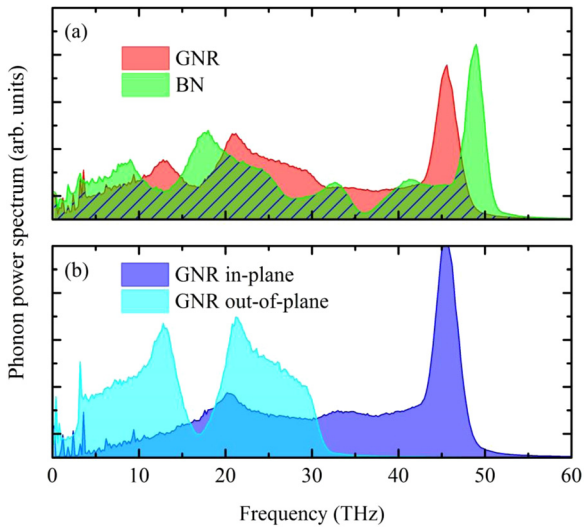

FIG. 4. (a) Phonon power spectra of GNR and h-BN. Overlap areas are denoted by the black line patterns. (b) In-plane and out-of-plane phonon spectrum decomposition in GNR.

GNR to h-BN. For the suspended structure, the flexural phonon mode has been proven to dominate the thermal transport in graphene and the in-plane and out-of-plane phonons are well decoupled.[40] With the existence of h-BN monolayer, various symmetry rules, i.e., reflection, transmission, and rotation are broken. The phonon vibrations in carbon atoms are affected by the interactions between GNR and h-BN. Since GNR is superposed on the substrate surface to match the honeycomb lattice, the boron and nitrogen atoms underneath will behave as scattering centers for the in-plane phonons in GNR, which unleashes the thermal energies stored in the in-plane phonons and transfers them into flexural phonon modes. This as a result strengthens the heat transfer between graphene and h-BN interfaces and reduces their thermal contract resistance.

Thermal relaxation time τ, which characterizes the time elapsed for the hybrid system to reach steady state again, is calculated for each case. The equation used to calculate τ is expressed as $\Delta T(t) = \Delta T(t_0)\exp[(t_0 - t)/\tau]$, where t_0 represents the start time of the simulation. Figure 3(b) shows the thermal relaxation time results for corresponding R values in Fig. 3(a). The relationship between R and τ reveals the underlying physical meaning of thermal boundary resistance, which indicates the efficiency of thermal transport across interfaces.

Effect of temperature on interfacial thermal resistance is explained by analyzing the phonon power spectral density (PSD) of GNR and h-BN, respectively, which can be calculated by taking the Fourier transform of the velocity autocorrelation function (VAF) $F(\omega) = 1/\sqrt{2\pi}\int_{-\infty}^{\infty} dt e^{iwt} Z(t)$, where $Z(t) = < v(0)\cdot v(t) > / < v(0)\cdot v(0) >$. Higher values of PSD for a phonon with frequency f means more states are occupied by it. And zero PSD means there is no phonon with frequency f exists in the system. The phonon power spectrum analysis provides a quantitative means to assessing the power carried by phonons in a system. Figure 4(a) shows that the phonon power spectrum results of GNR and h-BN. Due to the anisotropic thermal property of graphene, the in-plane and out-of-plane phone power spectra are calculated for GNR additionally, as are shown in Fig. 4(b). To better understand the calculation results, an arbitrary unit variable defined as $\delta = \int fA(f)df$, where $A(f)$ is the intersection area at frequency f, is computed.[41] $\delta|_0^{35}$ is calculated at 42.5 and $\delta|_{35}^{60}$ is 21.4. The area integration is proportional to the amount of energy transported across the interface by phonons at these frequency intervals. It is concluded that the majority of the phonon couplings occur at low frequencies below 35 THz, which is the active phonon frequency of flexural phonons shown in Fig. 3(b), while the in-plane phonons contribute at both low and high frequencies. As the system temperature increases, more high frequency phonons will become activated and start making contributions to the interfacial thermal transport. The phonon mean free path becomes shorter at a high temperature due to the higher number of phonons and an increased number of in-plane anharmonic phonon-phonon scattering events. The Umklapp scattering in lateral directions increases with temperature and boosts the phonon population at low frequencies, which directly enhances the thermal transport across interfaces.

C. Effects of heat flux direction

A better understanding of the interfacial heat conduction mechanism has led to potential interesting applications based on the possibility to control the heat flow. Thermal rectification in heterostructures has potential applications in nanoscale thermal management such as on-chip cooling and energy conversion by controlling the heat transport and is also fundamental in several novel schemes of thermal circuits and information processing using phonons.[42–45] Previous studies had investigated the thermal rectifications at graphene/carbon nanotube-based TIMs which are very promising for thermal rectifier applications.[16,46,47]

To create a reversed heat flux in the hybrid system, the ultrafast heat flux is imposed on the h-BN monolayer instead

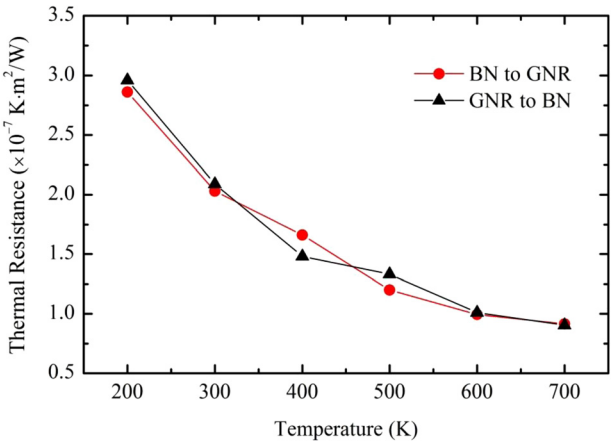

FIG. 5. Thermal rectification calculations at different temperatures.

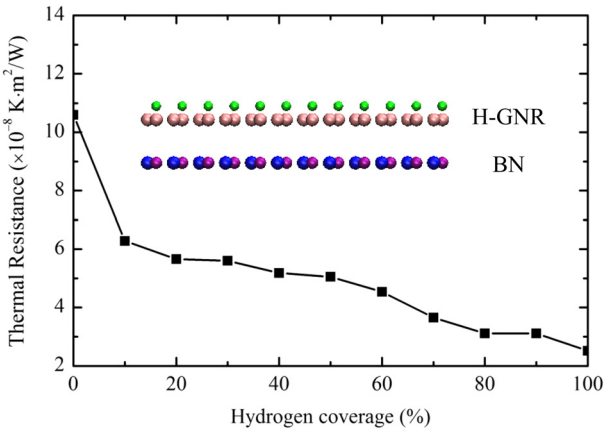

FIG. 6. Effects of hydrogenation on the thermal resistance between H-GNR and *h*-BN.

of GNR after the heterostructure reaches steady state. Thermal contact resistances are calculated at different temperatures for both heat flux directions, as is shown in Fig. 5. Interaction strength χ is set as 1 for all cases. Since the hybrid structure is placed in a thermal insulated environmental, the system's final temperature would be the same given the same amount of energy added to the system. Therefore, the same value of q_{in} is applied for each paired calculations. No obvious R differences are observed from the results in Fig. 5 and it is concluded that there is no thermal rectification at GNR/*h*-BN interfaces.

D. Effects of hydrogenation

Functionalization of graphene through chemical methods has attracted great interest and is explored recently due to the possibility of nanostructuring graphene into complex patterns.[48–50] Thermal properties of hydrogenated graphene (H-GNR) and oxidized graphene (O-GNR) have been investigated by previous studies in seeks of better thermal management and thermoelectric applications.[51–53] In this work, the effects of hydrogenation on thermal transport across GNR/*h*-BN interfaces are studied. To keep consist with the previous calculations, dimensions of the heterostructure remain unchanged and the transient heating technique is applied. Scaling parameter χ is set as 1 for all calculations and the final temperature of the hybrid system equals 600 K. Configuration of the H-GNR/*h*-BN system is shown in the inset of Fig. 6, where the hydrogen atoms are placed on top of the GNR structure. C-H bond length equals 1.125 Å. Although the hydrogen distribution patterns can affect the thermal properties of graphene, it would be impractical to consider all the scenarios. To simply the calculations, this work focuses on the effects of hydrogen coverage ratio on interfacial thermal transport and only one H-GNR formation is used. Hydrogen coverage ratio is defined as $\eta = M/N$, where M is the number of hydrogen atoms and N equals half the number of carbon atoms. Hydrogen coverage ratio is controlled by randomly adding/removing atoms.

Figure 6 shows that the interfacial thermal resistance R between H-GNR/*h*-BN decreases monotonically with η. The minimum value of R equals 2.51×10^{-8} K·m^2/W, which is 76.3% smaller than that of the pristine GNR/*h*-BN case. During the transient heating process of H-GNR, thermal energies are evenly added to each direction. Thus, two third of the thermal energies will be confined at the lateral direction and slowly releases to the out-of-plane direction. With the existence of hydrogen atoms, a new channel is opened for the in-plane and out-pf-plane phonon couplings in GNR which greatly enhances the interfacial thermal transport across the interfaces. The effects of hydrogenation are more influential at low coverages ratios and become weaker as the coverage ratio increases. This conclusion can be confirmed by Fig. 4(b) and Figs. 9(a)–9(c). It can be observed that when the hydrogen coverage increases from 0% to 20%, formations of the in-plane and out-of-plane phonon power spectrums changes significantly, whereas when the coverage ratio increases from 50% to 80%, changes in the power spectrums are less noticeable. Therefore, the calculated interfacial thermal resistance significantly decreases at low hydrogenating stage, while as the hydrogenating amount keep increasing, only slight decrease of R is observed. It has been proved in a previous study that impurities in graphene introduced by hydrogenation can greatly reduce its thermal conductivity by more than 70%.[53] And it is exciting to find out this impurity, on the other hand, can benefit the thermal transport across H-GNR/*h*-BN interfaces. In order to elucidate the underlying mechanism, the contributions of hydrogen and carbon atoms to thermal transport are calculated respectively. Interactions between H, C, and *h*-BN atoms are turned on/off by controlling the energy parameter ε_{C-BN} and ε_{H-BN} in the LJ potential. When ε_{C-BN} is set to zero, only hydrogen atoms' contributions are considered in the thermal transport, and likewise for ε_{H-BN}. Figure 7 shows the decomposed contributions from H and C atoms to the interfacial thermal transport. It can be observed that the profiles of ($\varepsilon_{C-BN} \neq 0$, $\varepsilon_{H-BN} = 0$) and ($\varepsilon_{C-BN} \neq 0$, $\varepsilon_{H-BN} \neq 0$) remain tightly close at most data points, which indicate carbons atoms make the majority of contributions to the thermal transport. The hydrogen atoms' contributions gradually increase with η as more hydrogen atoms are involved in the thermal transport process, which directly enhances the thermal energy transport across H-GNR/*h*-BN interfaces.

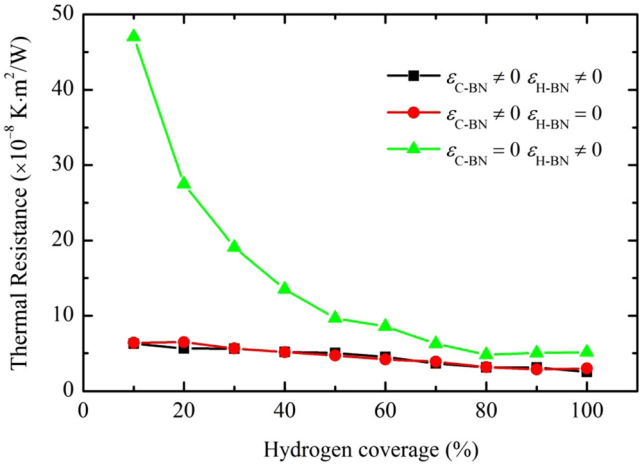

FIG. 7. Contributions of carbon and hydrogen atoms to the interfacial thermal resistance.

To gain further insight into this phenomenon, detailed analysis of the phonon spectrum under different H coverages is conducted on both hydrogen and carbon atoms. Plotted in Fig. 8 are the phonon power spectra for hydrogen atoms when η equals 20%, 50%, and 80% in H-GNR. The phonon spectrum shifts to right and becomes broader as η increases. The spectrum coverage areas become significant larger in the frequency of 40–50 THz, which is the major peak frequency of GNR as shown in Fig. 4(a) and indicates improved couplings between H and C. The deformation of phonon spectrum with η also facilitates the interfacial thermal transport due to the better match between H and BN atoms at broad moderate frequencies. It has been proved in previous studies that the decoupled nature of in-plane and out-of-plane phonons in graphene can lead to some extraordinary phenomena like co-existing heat currents, phonon energy inversion and negative effective thermal conductivity.[54,55] However, these novel thermal properties of graphene could impede the heat dissipation across graphene interfaces. In free standing graphene systems, the phonon coupling time between in-plane and out-of-plane phonons could be 4.7 times longer than that only between in-plane phonons.[55] This

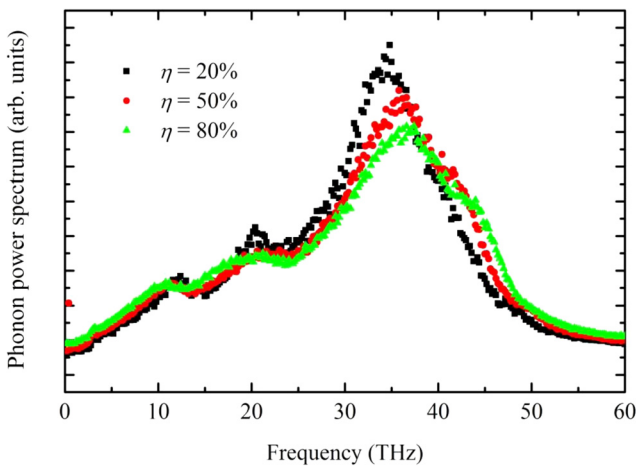

FIG. 8. Phonon power spectra of hydrogen atoms at different coverage ratios.

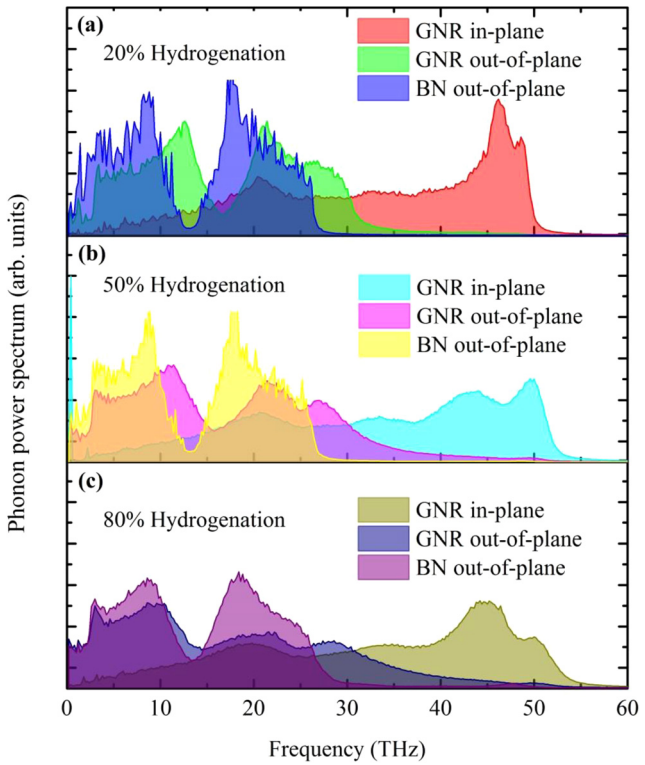

FIG. 9. Effects of hydrogenation on the in-plane and out-of-plane phonon power spectra of graphene and out-of-plane phonon power spectra of BN.

indicates the thermal energies are restrained in lateral directions and can only be slowly released to the flexural phonons. By hydrogenating graphene in the heterostructure, it has been observed that the couplings between in-plane and out-of-plane phonons have been greatly enhanced. Figures 9(a)–9(c) depict the in-plane and out-of-plane phonon power spectra of H-GNRs and out-of-plane phonon power spectrum of *h*-BN at 20%, 50%, and 80% hydrogen coverage. As the hydrogenation ratio increases, the overlap area between in-plane and out-of-plane phonons in H-GNR greatly increases. The improvement of in-plane and out-of-plane phonon couplings in graphene indirectly facilitates the thermal transport across interface and reduces the thermal contact resistances between H-GNR and *h*-BN. In the meantime, the PDOS of H-GNR becomes smoother and broader at higher η values, which directly strengthens the phonon couplings between H-GNR and *h*-BN. On the other hand, the overlap areas between H-GNR and *h*-BN's out-of-plane direction phonons are calculated by equation $\delta = \int fA(f)df$, which equals 62.9, 64, and 67.3, respectively, for 20%, 50%, and 80% hydrogen coverages. Therefore, the interfacial thermal resistance reduction between H-GNR and BN are contributed by two major factors: (1) enhanced couplings between in-plane and out-of-plane acoustic phonons in H-GNR and (2) stronger phonon couplings between H-GNR and BN in the out-of-plane direction.

IV. CONCLUSION

Classic MD simulation is performed in this work to study the interfacial thermal transport across graphene and *h*-BN interfaces. Thermal contact resistances are characterized

by a fast transient technique which follows the principles of the experimental pump-probe method. It has been proved that R values between GNR/h-BN do not have significant changes over the transient thermal relaxation process. The calculated R results decrease monotonically with temperature and bond strength, which are attributed to increased phonon populations and enhanced phonon couplings between layers. An efficient chemical functionalization approach to facilitate the heat dissipation across graphene and single layer hexagonal boron nitride interface is reported. It is discovered that the thermal contact resistance can be reduced by 76.3% by graphene hydrogenation. The hydrogen atoms behave as vibrational centers for the supported graphene nanoribbon, which enhances the in-plane and out-of-plane phonon couplings and broadens the phonon channels in GNR. This work provides a fundamental understanding of GNR and h-BN interfacial thermal transport and can be used to improve the nano-device performance in thermal engineering with optimized nanoscale chemical functionalization.

ACKNOWLEDGMENTS

National Natural Science Foundation of China (Nos. 51206124 and 51428603) and SRF for ROCS, SEM, and support of UNL Holland Computing Center are gratefully acknowledged.

[1]A. Bagri, S. P. Kim, R. S. Ruoff, and V. B. Shenoy, Nano Lett. **11**, 3917–3921 (2011).
[2]S. K. Chien, Y. T. Yang, and C. K. Chen, Carbon **50**, 421–428 (2012).
[3]J. N. Hu, S. Schiffli, A. Vallabhaneni, X. L. Ruan, and Y. P. Chen, Appl. Phys. Lett. **97**, 133107 (2010).
[4]C. Sevik, A. Kinaci, J. B. Haskins, and T. Cagin, Phys. Rev. B **84**, 085409 (2011).
[5]C. Sevik, A. Kinaci, J. B. Haskins, and T. Cagin, Phys. Rev. B **86**, 075403 (2012).
[6]S. K. Singh, M. Neek-Amal, S. Costamagna, and F. M. Peeters, Phys. Rev. B **87**, 184106 (2013).
[7]C. Y. Zhi, Y. Bando, C. C. Tang, H. Kuwahara, and D. Golberg, Adv. Mater. **21**, 2889–2893 (2009).
[8]Y. N. Yue, J. C. Zhang, and X. W. Wang, Small **7**, 3324–3333 (2011).
[9]Z. Chen, W. Jang, W. Bao, C. N. Lau, and C. Dames, Appl. Phys. Lett. **95**, 161910 (2009).
[10]B. Liu, J. A. Baimova, C. D. Reddy, S. V. Dmitriev, W. K. Law, X. Q. Feng, and K. Zhou, Carbon **79**, 236–244 (2014).
[11]B. Liu, J. A. Baimova, C. D. Reddy, A. W. K. Law, S. V. Dmitriev, H. Wu, and K. Zhou, ACS Appl. Mater. Interface **6**, 18180–18188 (2014).
[12]Z. Y. Wei, Z. H. Ni, K. D. Bi, M. H. Chen, and Y. F. Chen, Phys. Lett. A **375**, 1195–1199 (2011).
[13]L. Lindsay and D. A. Broido, Phys. Rev. B **84**, 155421 (2011).
[14]I. Jo, M. T. Pettes, J. Kim, K. Watanabe, T. Taniguchi, Z. Yao, and L. Shi, Nano Lett. **13**, 550–554 (2013).
[15]S. S. Chen, A. L. Moore, W. W. Cai, J. W. Suk, J. H. An, C. Mishra, C. Amos, C. W. Magnuson, J. Y. Kang, L. Shi, and R. S. Ruoff, ACS Nano **5**, 321–328 (2011).
[16]J. N. Hu, X. L. Ruan, and Y. P. Chen, Nano Lett. **9**, 2730–2735 (2009).
[17]G. Wu and B. W. Li, Phys. Rev. B **76**, 085424 (2007).
[18]A. K. Vallabhaneni, B. Qiu, J. N. Hu, Y. P. Chen, A. K. Roy, and X. L. Ruan, J. Appl. Phys. **113**, 064311 (2013).
[19]S. Plimpton, J. Comput. Phys. **117**, 1–19 (1995).
[20]D. W. Brenner, O. A. Shenderova, J. A. Harrison, S. J. Stuart, B. Ni, and S. B. Sinnott, J. Phys.: Condens. Matter **14**, 783–802 (2002).
[21]B. W. Dodson, Phys. Rev. B **35**, 2795–2798 (1987).
[22]J. Tersoff, Phys. Rev. Lett. **61**, 2879–2882 (1988).
[23]L. Lindsay and D. A. Broido, Phys. Rev. B **81**, 205441 (2010).
[24]A. Kinaci, J. B. Haskins, C. Sevik, and T. Cagin, Phys. Rev. B **86**, 115410 (2012).
[25]A. K. Rappe, C. J. Casewit, K. S. Colwell, W. A. Goddard, and W. M. Skiff, J. Am. Chem. Soc. **114**, 10024–10035 (1992).
[26]A. H. Castro Neto, F. Guinea, N. M. R. Peres, K. S. Novoselov, and A. K. Geim, Rev. Mod. Phys. **81**, 109–162 (2009).
[27]L. Liu, Y. P. Feng, and Z. X. Shen, Phys. Rev. B **68**, 104102 (2003).
[28]Y. D. Ma, Y. Dai, M. Guo, C. W. Niu, and B. B. Huang, Nanoscale **3**, 3883–3887 (2011).
[29]N. T. Cuong, M. Otani, and S. Okada, Phys. Rev. Lett. **106**, 106801 (2011).
[30]G. Giovannetti, P. A. Khomyakov, G. Brocks, P. J. Kelly, and J. van den Brink, Phys. Rev. B **76**, 073103 (2007).
[31]K. Kamiya, N. Umezawa, and S. Okada, Phys. Rev. B **83**, 153413 (2011).
[32]M. H. Kang, S. C. Jung, and J. W. Park, Phys. Rev. B **82**, 085409 (2010).
[33]B. Lee, S. Han, and Y. S. Kim, Phys. Rev. B **81**, 075432 (2010).
[34]D. G. Cahill, K. E. Goodson, and A. Majumdar, Trans. ASME J. Heat Transfer **124**, 223–241 (2002).
[35]Z. Y. Ong and E. Pop, Phys. Rev. B **81**, 155408 (2010).
[36]C. F. Carlborg, J. Shiomi, and S. Maruyama, Phys. Rev. B **78**, 205406 (2008).
[37]J. Zhang, Y. Wang, and X. Wang, Nanoscale **5**, 11598–11603 (2013).
[38]C. C. Chen, Z. Li, L. Shi, and S. B. Cronin, Appl. Phys. Lett. **104**, 081908 (2014).
[39]A. Mattausch and O. Pankratov, Phys. Rev. Lett. **99**, 076802 (2007).
[40]L. Lindsay, D. A. Broido, and N. Mingo, Phys. Rev. B **82**, 115427 (2010).
[41]M. Li, J. Zhang, X. Hu, and Y. Yue, "Thermal transport across graphene/SiC interface: effects of atomic bond and crystallinity of substrate," Appl. Phys. A (published online).
[42]B. W. Li, L. Wang, and G. Casati, Appl. Phys. Lett. **88**, 143501 (2006).
[43]L. Wang and B. Li, Phys. Rev. Lett. **99**, 177208 (2007).
[44]B. W. Li, L. Wang, and G. Casati, Phys. Rev. Lett. **93**, 184301 (2004).
[45]L. Wang and B. W. Li, Phys. Rev. Lett. **101**, 267203 (2008).
[46]A. Rajabpour, S. M. V. Allaei, and F. Kowsary, Appl. Phys. Lett. **99**, 051917 (2011).
[47]X. L. Zhang, M. Hu, and D. W. Tang, J. Appl. Phys. **113**, 194307 (2013).
[48]T. Kuila, S. Bose, A. K. Mishra, P. Khanra, N. H. Kim, and J. H. Lee, Prog. Mater. Sci. **57**, 1061–1105 (2012).
[49]D. W. Boukhvalov and M. I. Katsnelson, J. Phys.: Condens. Matter **21**, 344205 (2009).
[50]A. K. Singh and B. I. Yakobson, Nano Lett. **9**, 1540–1543 (2009).
[51]H. J. Zhang, A. F. Fonseca, and K. Cho, J. Phys. Chem. C **118**, 1436–1442 (2014).
[52]J. Y. Kim, J. H. Lee, and J. C. Grossman, ACS Nano **6**, 9050–9057 (2012).
[53]S. K. Chien, Y. T. Yang, and C. K. Chen, Appl. Phys. Lett. **98**, 033107 (2011).
[54]J. C. Zhang, X. W. Wang, and H. Q. Xie, Phys. Lett. A **377**, 2970–2978 (2013).
[55]J. C. Zhang, X. W. Wang, and H. Q. Xie, Phys. Lett. A **377**, 721–726 (2013).